Biophysical Chemistry, 30 (1988) 257–269
Elsevier

BPC 01263

Brownian dynamics simulations of intramolecular energy transfer

Jeffrey W. Berger and Jane M. Vanderkooi

Department of Biochemistry and Biophysics, School of Medicine, University of Pennsylvania, Philadelphia, PA 19104, U.S.A.

Received 25 January 1988
Accepted 23 March 1988

Energy transfer; Rotational diffusion; Brownian dynamics; Fluorescence anisotropy

A novel technique for modelling intramolecular energy transfer is presented. Brownian dynamics calculations are used to compute the trajectories of donor and acceptor species, and the instantaneous orientation factor is calculated during each temporal iteration. In this work, several model systems are considered. Trajectories were computed for energy transfer between a flexible donor and a rigidly fixed acceptor. We have considered configurations where the donor is, (1) tethered to a fixed point in space, but free to diffuse rotationally, and (2) constrained to wobble in a cone. The luminescence decay of the donor is 'measured', and a non-single-exponential decay is observed for configurations of efficient energy transfer. Luminescence anisotropy measurements of constrained and unconstrained donors reflect the contribution of both energy transfer and rotational diffusion to the shape of the anisotropy decay curve.

1. Introduction

It is well known that inter- and intramolecular energy-transfer processes can be efficient over distances less than 70 Å [1]. The theory describing the interaction between donor and acceptor moieties in the weak dipole-dipole limit was first put forth by Förster [2] in 1948. As energy transfer in the Förster regime depends on both the separation and alignment of the donor (D) and acceptor (A) species, distance and orientation information can be extracted from energy-transfer measurements.

While the efficiency of Förster energy transfer has been used to quantify the donor-acceptor separation, the relative orientation between the donor and acceptor needs to be considered. The influence of the orientational factor on the energy-transfer efficiency has been discussed previously [1,3,4], and it is postulated that the uncertainty introduced by an unknown orientation factor is less than 20%. In general, it is assumed that the time scale for energy transfer is longer than that for fluorophore (luminophore, in general) motion. Specifically, the donor/acceptor is assumed to sample all available orientations during energy transfer. If both the donor and the acceptor are unconstrained, then $\langle k^2 \rangle = 2/3$ where $\langle k^2 \rangle$ is the ensemble average of the orientation factor. Similarly, if the donor or acceptor is constrained to 'wobble-in-a-cone', then all orientations are sampled within the energy-transfer time scale, and $\langle k^2 \rangle$ can be deduced. Dale and Eisinger [5] have considered a large number of donor-acceptor geometries, and the orientation factor is determined for each configuration subject to the simplification described above.

The accumulation of protein crystallographic data allows for verification of energy-transfer measurements. In particular, theory and experiment can be compared in order to assess the accuracy of energy transfer as a 'spectroscopic ruler.' Further, the assumptions made in the early energy-transfer literature can be evaluated.

Correspondence address: J.M. Vanderkooi, Department of Biochemistry and Biophysics, School of Medicine, University of Pennsylvania, Philadelphia, PA 19104, U.S.A.

We have developed a computer simulation of intramolecular energy transfer in order to improve our understanding of energy-transfer measurements, and as a tool to be used in the interpretation of experimental observations. Several model systems are analyzed in order to evaluate the effectiveness of the simulation technique. In this work, we simulate the dynamics of a flexible fluorophore in the vicinity of a rigidly fixed acceptor species. The lifetime of the donor emission and the luminescence anisotropy are 'measured.' Since donor wobble will affect both luminescence decay (through a time-varying orientational factor) and anisotropy decay (via energy transfer and Brownian rotational diffusion), it is of interest to study the combined effects of rotational diffusion and energy transfer, particularly when they occur on a similar time scale. This work differs from previous studies in that we are able to consider the most interesting temporal regime where energy transfer and rotational diffusion occur simultaneously.

2. Theory

2.1. Energy transfer

The rate constant for energy transfer is given by,

$$K_{ET} = (1/t_D)(R_0^6/R_{DA}^6) \quad (1)$$

where t_D is the emission lifetime of the donor in the absence of the acceptor, R_{DA} the donor-acceptor separation, and R_0 the Förster characteristic separation, i.e., the distance where the probability of energy transfer is equal to the probability of deactivation by other processes. We can express the characteristic separation,

$$R_0^6 = Ck^2 \quad (2)$$

where C is a constant dependent on the quantum yield of the donor, the index of refraction of the intervening medium, and the spectral overlap between donor emission and acceptor excitation spectra. The orientation factor is defined as

$$k^2 = (\cos\alpha - 3(\cos\beta)(\cos\gamma))^2 \quad (3)$$

where α is the angle between the donor and acceptor, and β and γ those between the separation vector and the donor and acceptor, respectively [4].

2.2. Rotational diffusion

Theoretical treatments of rotational diffusion abound in the literature. Based on theory originally put forth by Perrin [6,7], and later refined by Weber [8], Favro [9], Tao [10] and Belford et al. [11], the relation between the size and shape of a freely rotating particle, and the emission anisotropy decay has been determined. Belford et al. [11] have shown that the anisotropy associated with an arbitrarily shaped body will decay with as many as five exponential time constants. For a sphere, the anisotropy decays as a single exponential,

$$A(t) = 0.2(3\cos^2\lambda - 1)\exp(-6D_{rot}t) \quad (4)$$

where λ is the angle between the absorption and emission dipole moments and D_{rot} the rotational diffusion coefficient [12]. The diffusion coefficient is simply a function of particle size and solvent conditions,

$$D_{rot} = (kT/6\eta V) \quad (5)$$

where k is Boltzmann's constant, T the absolute temperature, η the solvent viscosity and V the volume of the particle.

Rotational diffusion subject to conical constraints has been studied to interpret depolarization measurements of membrane-bound fluorophores, and as a model for macromolecular internal dynamics [13–16]. Lipari and Szabo [15] derived closed-form analytical approximations to the correlation function for diffusion in a 'hard-cone' potential well, while Kinosita et al. [14] and Szabo [17] have conducted analyses of continuous potential functions. The results of wobbling-in-a-cone simulations subject to energy transfer will be compared to analytical and numerical calculations of rotational diffusion in the absence of energy transfer.

2.3. Brownian dynamics

The traditional approach to the analysis of diffusion processes is to solve the associated deterministic diffusion equation. For rotational diffusion of a sphere [18],

$$\frac{\partial W}{\partial t}(\theta,\phi,t) = D_{\text{rot}}\nabla^2 W(\theta,\phi,t) \tag{6}$$

where W is the probability that the sphere is oriented at (θ,ϕ) at time t. Whereas solution of the diffusion equation requires a detailed knowledge of global inhomogeneities (spatial gradients), the Markovian nature of Brownian diffusion allows the trajectories to be computed by considering only local conditions [19].

The Langevin equation describes the balance of forces for a Brownian particle [20]. Solutions to the stochastic differential equations describing diffusive behavior have led to the development of Brownian dynamics techniques which have been used to study bimolecular diffusion [21], internal protein dynamics [22], protein folding [23], enzyme-substrate association [24], rotational diffusion [25] and other stochastic phenomena. We simulate the Brownian rotational diffusion of an excited fluorophore subject to Förster energy transfer.

2.4. Governing equations

In this work, we consider a system consisting of a flexible donor and a rigidly fixed acceptor. Appropriate terms are added to the diffusion equation to include the effects of radiative emission and energy transfer [26]. The populations of excited donors, W_{D}, and excited acceptors, W_{A}, are described by eqs. 7 and 8,

$$\frac{\partial W_{\text{D}}}{\partial t} = D_{\text{rot}}\nabla^2 W_{\text{D}}(\theta,\phi,t) - \left(k_{0\text{D}} + K_{\text{ET}}(\theta,\phi)\right)W_{\text{D}}(\theta,\phi,t) \tag{7}$$

$$\frac{\partial W_{\text{A}}}{\partial t} = K_{\text{ET}}(\theta,\phi)W_{\text{D}} - k_{0\text{A}}W_{\text{A}} \tag{8}$$

where $k_{0\text{D}}$ and $k_{0\text{A}}$ are the rate constants for emission from the donor and acceptor excited states, D_{rot} the rotational diffusion coefficient, θ and ϕ the spherical coordinates of the donor emission moment, and K_{ET} the rate constant for energy transfer which is dependent on the instantaneous position of the donor.

The first term on the right-hand side of eq. 7 is the diffusive contribution. The second term describes the dissipative processes of natural radiative decay and energy transfer. Eq. 8 has no diffusive term, since the acceptor is assumed to be rigidly fixed. In addition, the energy transfer term is positive, since the forward ($\text{D} \rightarrow \text{A}$) transfer mechanism is heavily favored over the reverse process. Finally, the acceptor will emit with its own characteristic rate constant.

Eqs. 7 and 8 are a pair of coupled, partial differential equations; if the populations of both excited donors and excited acceptors were of interest, then eqs. 7 and 8 would have to be solved simultaneously. In this work, we consider only measurements of the donor emission, hence we solve for W_{D}. The calculations are simplified, since eq. 7 has no explicit W_{A} dependence.

3. Method

The equations governing energy transfer have been solved both analytically [26–29] and numerically [30], for specific geometries. We implement a Brownian dynamics simulation in order to include many of the complexities that could not be considered in past treatments. In addition, simulation techniques offer flexibility that will enable us to consider a wide variety of donor-acceptor configurations and dynamical constraints.

We have developed software in our laboratory to model the luminescence anisotropy decay experiment. Brownian dynamics techniques [25,31, 32] are used to simulate the rotational diffusion associated with overall macromolecular tumbling and local segmental flexibility. The simulation follows the trajectories of N identical particles subject to Brownian rotational diffusion. Dynamical calculations are performed in the molecular coordinate system while a Euler-like rotation tensor [33] allows for transformation between the body and laboratory coordinate systems. Complete trajectories are calculated through temporal iteration.

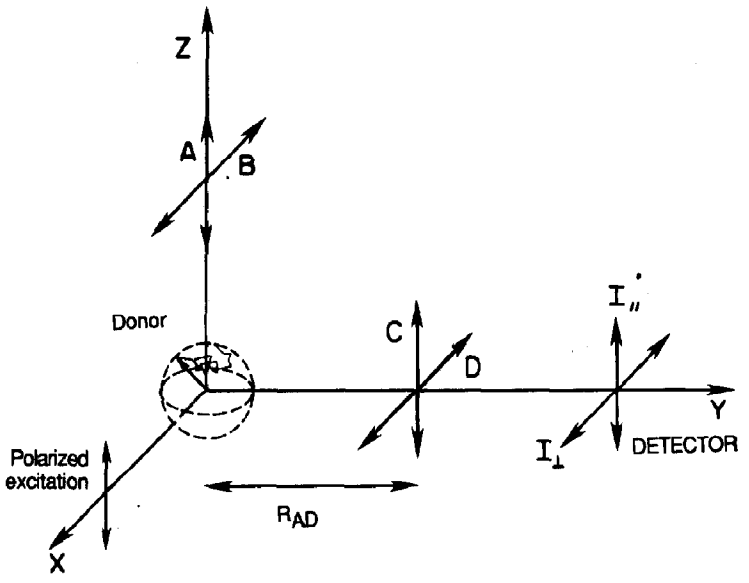

Fig. 1. The geometry. The donor is fixed to the origin, but free to diffuse rotationally. The four acceptors are labelled, A (case 1), B (case 2), C (case 3) and D (case 4). The center-to-center separation between the donor and each of the acceptors is R_{DA}.

Two models are considered for donor motion. First, we model the donor as tethered to a fixed point in space, but free to diffuse rotationally. Next, we consider the more physically relevant model of a dipole wobbling in a cone of semiangle θ_c. Recent studies have considered various constraining potential wells, however, it has been suggested that the choice of model is not critical provided the motion is bounded by a conical constraint [14]. For simplicity, we have chosen the hard-cone potential where the fluorophore is free to move in a potential well such that $V = 0$ for $\theta < \theta_c$ and $V = \infty$ for $\theta > \theta_c$.

Energy transfer is included by calculating the instantaneous energy transfer rate, $K_{ET}(k)$, for each particle. The energy-transfer efficiency is a function of the instantaneous orientation factor, and this is determined at each time step for each particle in the simulation.

We consider the geometry depicted in fig. 1. Vertically polarized light photoselects a fraction of donor fluorophores which are then free to diffuse rotationally. The donor species can lose energy in two ways, (1) natural radiative decay with a rate constant of $K_0 = 1/t_0$, and (2) energy transfer with a rate constant $K_{ET}(k)$, dependent on the instantaneous orientation factor.

We can describe the time rate of change of the population of excited states, N^*, by

$$dN^*/dt = -(K_0 + K_{ET}(k))N^*. \tag{9}$$

The simulations were set up such that the lifetime of the excited species is 5 ns, while that of energy transfer is 3 ns (for $k^2 = 1$) – corresponding to rate constants of 2.0×10^8 and 3.3×10^8 s^{-1}, respectively. During each time increment, the instantaneous value for k^2 is computed for each particle, and the change in the number of excited donors is calculated.

The parallel (I_p) and perpendicular (I_s) components of the emitted light are 'measured', and both the overall emission intensity, $S(t)$, and the anisotropy, $A(t)$, can be determined,

$$S(t) = I_p(t) + 2I_s(t) \tag{10}$$

$$A(t) = (I_p(t) - I_s(t))/S(t). \tag{11}$$

In this work, we follow the trajectories of 200 particles for 100 temporal iterations, i.e., 20 ns. All simulations were conducted on an ATT

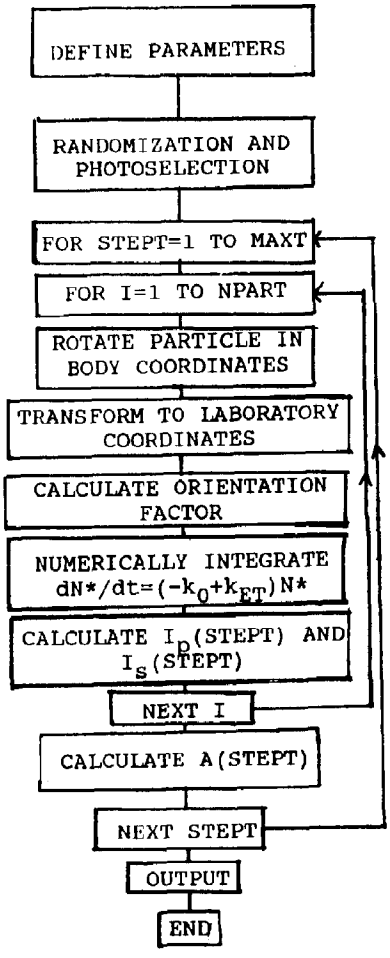

Fig. 2. Flow chart of the computer simulation.

PC6300 personal computer and the computation time for each trajectory was 2 h. A flow chart of the simulation program has been included (fig. 2).

4. Results and discussion

We calculate the intensity decay of a donor undergoing Brownian rotational diffusion at a distance R_{DA} from an acceptor species in order to evaluate the efficiency of energy transfer in various configurations. Considerable insight can be obtained by considering very simple geometries. We consider cases where the acceptor is parallel or perpendicular to the direction of photoselection. In addition, we can specify the acceptor to be parallel or perpendicular to the imaginary line joining the donor and the acceptor. The results of luminescence decay and anisotropy decay experiments are simulated for each of the four configurations depicted in fig. 1. Trajectories were computed for both constrained and unconstrained donors.

4.1. Donor luminescence decay

4.1.1. Unconstrained donor

The luminescence decay of an unconstrained donor transferring energy to each of the four acceptor species is depicted in fig. 3. The effi-

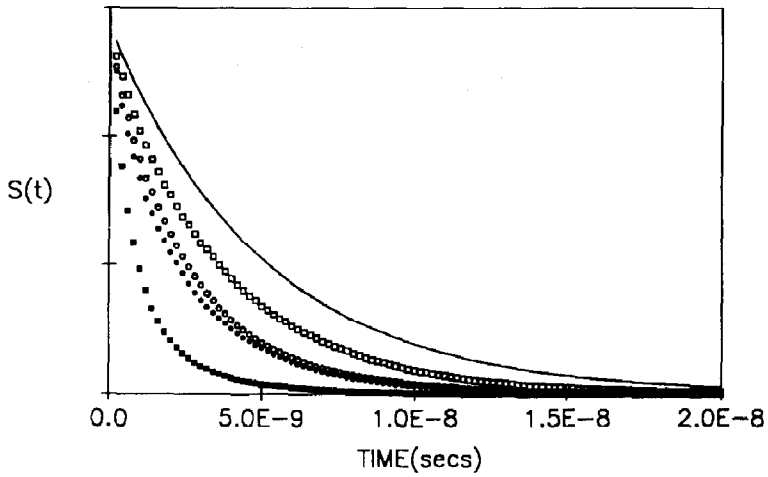

Fig. 3. Luminescence decay for the unconstrained donor. Raw data as derived from the simulations for case 1 (■), case 2 (●), case 3 (○) and case 4 (□). The solid line depicts the intensity decay in the absence of energy transfer.

ciency of energy transfer varies in the four experiments that have been simulated. Clearly, energy transfer is most efficient when the acceptor is parallel to both the photoselection direction and the line joining the donor and acceptor (case 1), while the least efficient energy transfer occurs when the acceptor dipole is perpendicular to both the photoselection direction and the donor-acceptor line (case 4).

The two intermediate cases present an interesting paradox. Photoselection dictates that the excited donors will be preferentially aligned with the z-axis at $t = 0$. Since energy transfer is most efficient between aligned dipoles, one would expect energy transfer to be more efficient in case 3 than in case 2 – particularly at short times, before the distribution of excited donors is allowed to equilibrate. Our simulations contradict this notion. Energy transfer is nearly equally efficient in cases 2 and 3 with transfer being slightly more efficient in case 2. This finding is somewhat counter-intuitive. The discrepancy can be resolved by noting that energy transfer is a function of both the alignment of the dipoles and the relationship between the transition moments and the separation vector, $\boldsymbol{R}_{AD}$. Energy transfer is most efficient when the donor and acceptor are aligned along the separation vector, hence the similar efficiency in cases 2 and 3 is a product of two competing effects. In case 2, the alignment of the donor with $\boldsymbol{R}_{AD}$ will result in increased efficiency while the orientation of the acceptor normal to the photoselection direction will tend to reduce the efficiency. Similarly, the alignment of the acceptor in case 3 with the z-axis will tend to favor energy transfer, while the orientation of the acceptor perpendicular to the separation vector will limit the energy-transfer efficiency.

The luminescence decay curves were fitted to solve for the effective rate constant,

$$K_{\text{eff}} = K_0 + \langle k^2 \rangle_{\text{eff}} K_{\text{ET}}. \tag{12}$$

Since the rate constants associated with both the natural radiative lifetime and the energy-transfer mechanism are known, the effective orientation factor can be extracted (table 1).

If the ensemble average of the orientation factor is constant over the duration of the simulation, then the decay of the emission will be monoex-

Table 1

Effective orientation factor for unconstrained donors

Case	$\langle k^2 \rangle_{\text{eff}}$
1	2.10
2	0.63
3	0.55
4	0.22

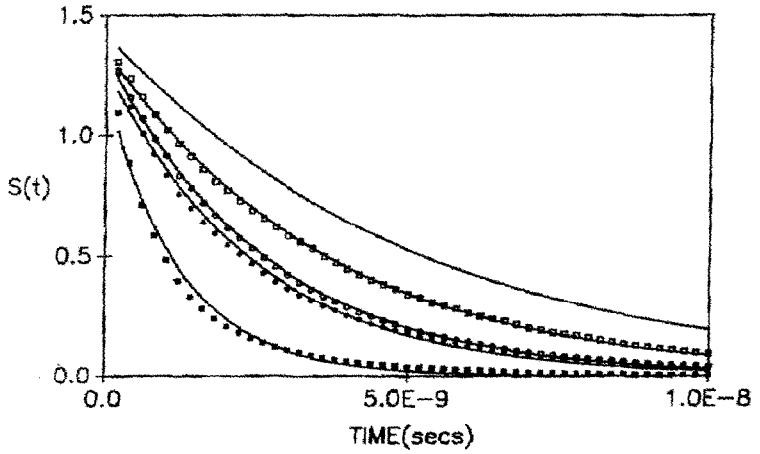

Fig. 4. Best monoexponential fit to the luminescence decay for an unconstrained donor. Single-exponential fits to the raw data are plotted for case 1 (■), case 2 (●), case 3 (○) and case 4 (□). The upper solid line is the intensity decay in the absence of energy transfer.

ponential. Alternatively, we expect a non-single-exponential decay for a process involving a time-dependent orientation factor. Molecular dynamics simulations [34] and direct picosecond measurements [35] of tryptophan-heme energy transfer in myoglobin report non-single-exponential decay of the tryptophan fluorescence. This result was interpreted to be indicative of the fluctuations in the relative orientation between the heme and the tryptophan on the energy-transfer time scale. An analogous effect is observed in our simulations.

The raw data for cases 1–4 are plotted in fig. 4 along with the best monoexponential fit. A good agreement exists between the fit and the raw data in case 4, however the 'goodness' of the fit deteriorates with increasing energy-transfer efficiency; the raw data for case 1 are clearly non-single exponential. The data of Hochstrasser and

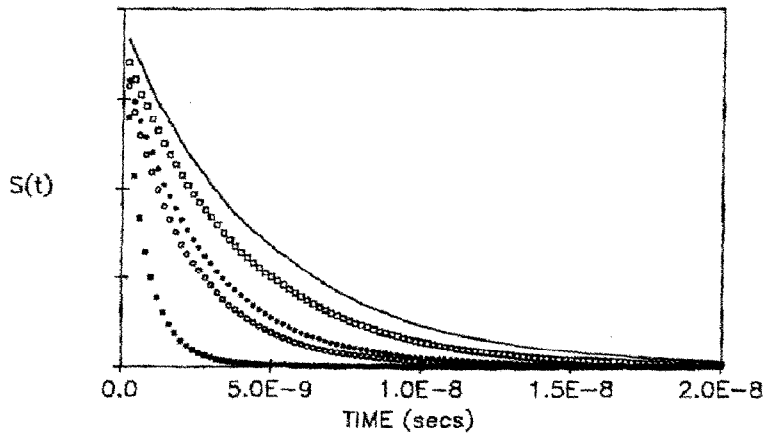

Fig. 5. Luminescence decay for a donor constrained to wobble in a hard cone of semiangle 45°. Raw data are plotted for case 1 (■), case 2 (●), case 3 (○) and case 4 (□).

his co-workers can be understood by realizing that the energy-transfer process in myoglobin is highly efficient. The principal tryptophan lifetime in the apoprotein is approx. 1 ns, while a lifetime of 15–30 ps is reported for the holoprotein [35]. In agreement with our data, the emission of a donor participating in a highly efficient energy-transfer process is nonexponential. The effective rate constant is the sum of those associated with the natural lifetime and energy transfer. For weak energy transfer, K_0 still dominates the deactivation equation, and the emission remains nearly monoexponential. For increasing K_{ET}, the effective rate constant assumes a stronger time dependence, and therefore a nonexponential luminescence decay is observed. Hence, the donor emission will deviate significantly from a single exponential as energy transfer becomes the principal deactivation process.

4.1.2. Constrained donor

The dynamical behavior of a fluorophore should not affect its emission lifetime, hence in the absence of energy transfer, the luminescence decay curves for the constrained and unconstrained donors are identical. Energy-transfer mechanisms remove this degeneracy.

We now consider the constrained donor. The luminescence decay curves for cases 1–4 are presented in fig. 5. Although the figure is quite similar to fig. 3, we note several distinctions. First, the relative positions of the decay curves for cases 2 and 3 are inverted. Whereas case 2 was the more efficient energy-transfer configuration for an unconstrained donor, case 3 becomes more efficient if the donor is constrained to wobble in a cone of 45°. Second, the overall decay rate associated with each of the configurations has changed. The luminescence decay curves were fitted to a single exponential in order to extract the effective orientation factor (table 2). These values are compared with those in table 1. In cases 1 and 3, the acceptor is aligned parallel to the z-axis. Since the conical constraint restricts the donors to wobble in the neighborhood of the z-axis, the effective orientation factor is greater than in the unconstrained case. Alternatively, the donors are prevented from achieving a preferred alignment in cases 2 and 4, hence $\langle k^2 \rangle_{eff}$ is reduced.

Table 2

Effective orientation factor for donors constrained to wobble in a cone of semiangle 45°

Case	$\langle k^2 \rangle_{eff}$
1	3.18
2	0.49
3	0.72
4	0.16

The inversion in the effectiveness of energy transfer for cases 2 and 3 can now be understood. Energy transfer in case 3 is made more efficient by constraining the donors to wobble in the vicinity of an axis parallel to the acceptor dipole moment. Case 2 is less efficient, since the donor is restricted from preferred orientations. Clearly, the relationship between the efficiencies of cases 2 and 3 is a function of θ_c. For the unconstrained donor, energy transfer is more efficient in case 2. Alternatively, a very narrow conical constraint will heavily favor energy transfer in case 3.

4.2. Depolarization of the donor luminescence

In order to discriminate between configurations of equally efficient energy transfer, we measure the polarization of the donor luminescence. In the absence of energy transfer, depolarization is due exclusively to the random rotational diffusion of the donor. In general, an acceptor will couple to both the parallel and perpendicular components of the donor emission. Since the interactions need not be equivalent, we expect to observe an anisotropy different from the measured anisotropy in the absence of energy transfer.

4.2.1. Unconstrained donor

Let us consider cases 2 and 3 for an unconstrained donor. With the acceptor parallel to the z-axis, the donors aligned with the z-axis should couple more strongly to the acceptor than donors near the x-y plane. In this way, the parallel emission will decay faster than the perpendicular emission, resulting in a net depolarization. Alternatively, an acceptor species parallel to the x-y

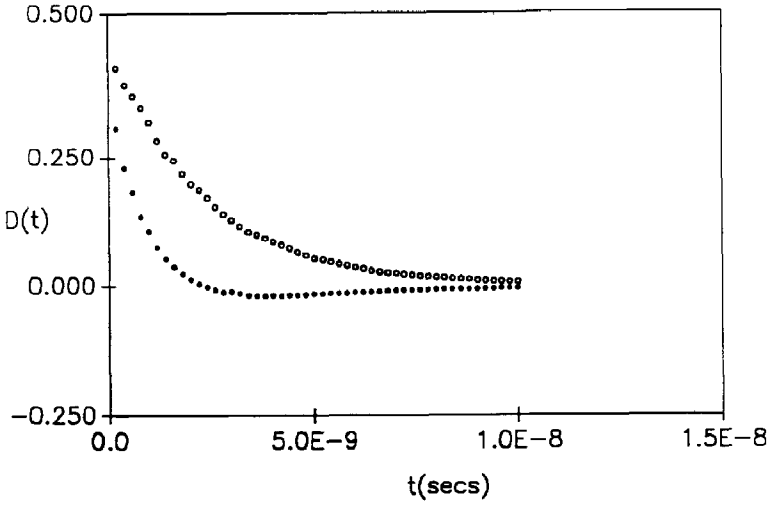

Fig. 6. Depolarization of the unconstrained donor luminescence. $D(t) = I_p - I_s$. Data are presented for case 2 (○) and case 3 (●).

plane will degrade the perpendicular intensity more strongly (on average) than the parallel intensity, yielding a net repolarization. This phenomenon is verified in fig. 6. Depolarization measurements, therefore, can be used to distinguish between different configurations having similar luminescence intensity decay behavior.

The contribution of energy-transfer mechanisms to luminescence depolarization has been previously described, however no evidence has been presented to account for repolarization due to energy-transfer processes. Our simulations suggest that repolarization will occur in specific configurations. This effect is understood in terms of 'intrinsic photoselection.' Polarized photoselection at $t = 0$ selects a population of excited donors preferentially aligned with the z-axis. An acceptor species parallel to the x-y plane will act to preserve this preferred alignment. While diffusive processes will tend to equilibrate the distribution of excited donors, energy-transfer processes will become more efficient (on average) as the donor

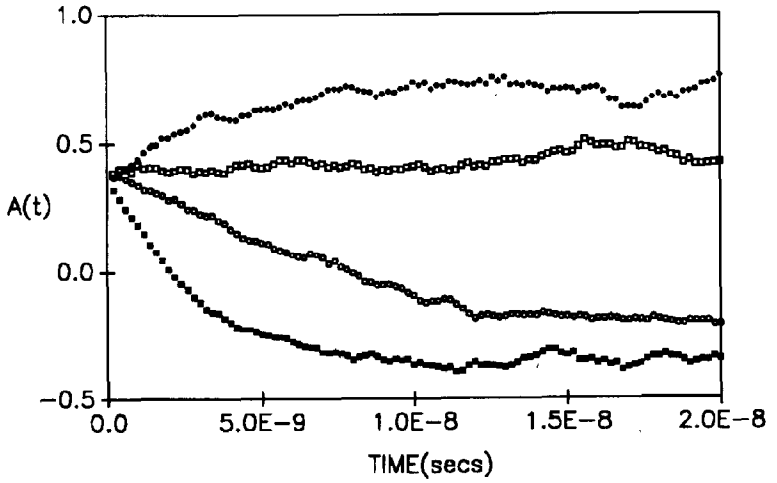

Fig. 7. Luminescence anisotropy decay for the unconstrained donor. Case 1 (■), case 2 (●), case 3 (○) and case 4 (□).

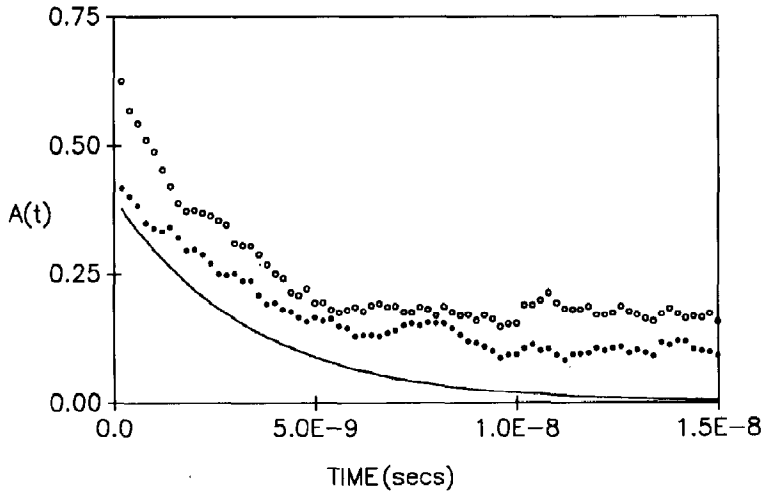

Fig. 8. Anisotropy decay for a constrained donor in the absence of energy transfer. Trajectories are presented for donors restricted to wobble in a 45° cone (○), a 75° cone (●) and for an unconstrained donor (solid line).

emission dipole approaches the x-y plane, hence the preferred alignment is maintained.

Anisotropy measurements of cases 1–4 for an unconstrained donor support this notion (fig. 7). The bottom curve of fig. 7 corresponds to case 1. The acceptor dipole moment is aligned parallel to the z-axis and along the donor-acceptor line. Energy transfer is most efficient, and those donors aligned with the z-axis preferentially couple with the acceptor, resulting in a rapid depolarization. While photoselection at $t = 0$ selects for donor molecules whose dipole moment is parallel with the z-axis, the acceptor species acts to annihilate these donors, preserving those in the x-y plane. The anisotropy passes through $A(t) = 0$ and assumes negative values, demonstrating that the parallel orientation has become unfavorable. Alternatively, the upper curve of fig. 7 (case 2) depicts a repolarization. As diffusion tends to equilibrate the photoselected distribution, energy transfer acts to maintain the preferred alignment. Indeed, energy transfer in case 2 favors a more sharply aligned distribution than initial photoselection, and the anisotropy rises above $A(t) = 0.4$.

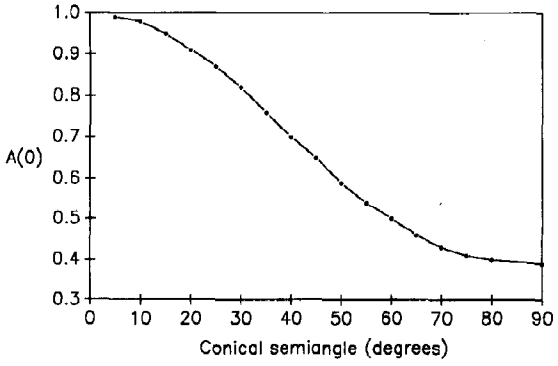

Fig. 9. Dependence of A_0 on the conical semiangle. Simulated results for the initial anisotropy of an ensemble of donors constrained to wobble in a hard cone.

We can determine the absolute limits for the anisotropy,

$$A(t) = (I_p - I_s)/(I_p + 2I_s) \tag{13}$$

$$\lim_{I_s \to 0} A(t) = 1 \tag{14}$$

$$\lim_{I_p \to 0} A(t) = -0.5. \tag{15}$$

In theory, a highly efficient energy-transfer process will annihilate one subpopulation of donors, and these limits will be achieved. The limiting values (for large t) of the anisotropy curves reflect the range of transfer efficiencies. Interestingly, the limiting anisotropy is determined by the competition between energy-transfer and diffusive processes. In the limit of very slow rotational

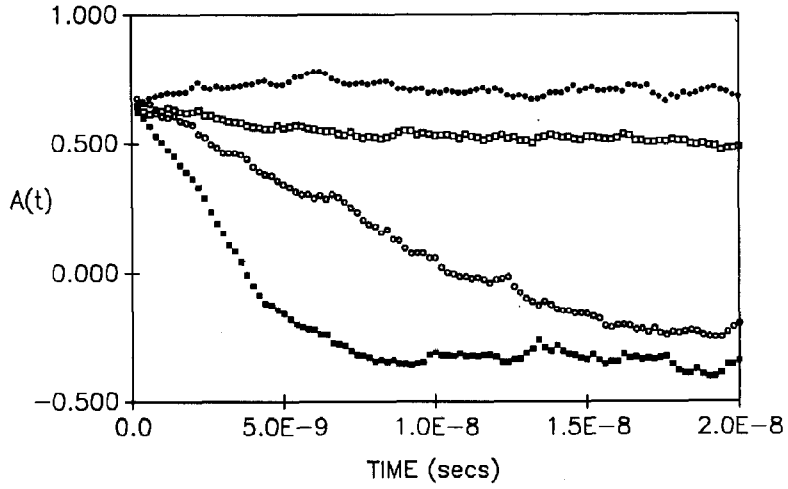

Fig. 10. Anisotropy decay for a donor constrained to wobble in a hard cone with semiangle 45°. Case 1 (■), case 2 (●), case 3 (○) and case 4 (□).

diffusion, energy transfer will selectively annihilate one population, while more rapid diffusion will allow re-equilibration. For example, in the rapid diffusion limit, excited dipoles aligned with the z-axis will rotate to the x-y plane before energy transfer can occur, resulting in a less aligned distribution.

The competition between rotational diffusion and energy transfer is reflected in case 4 (fig. 7) where the anisotropy remains nearly constant over the duration of the simulation. Diffusive processes tend to broaden the photoselected distribution, while an acceptor in the x-y plane acts to preserve the alignment. The nearly constant anisotropy suggests that the two processes act with equal and opposite strength.

4.2.2. Constrained donor

The anisotropy of a fluorescent species wobbling in a cone will be qualitatively different from that of a freely diffusing fluorophore. For an oriented sample and in the absence of energy transfer, we verify that both the initial and limiting values of the anisotropy (A_0 and $A_{\lim}$) are functions of the conical angle (fig. 8).

Kinosita et al. [13] asserted that the degree of confinement is a function of $A_{\lim}/A_0$. While the dynamical constraints can be derived for an isolated luminophore, we have demonstrated that the limiting anisotropy (and therefore $A_{\lim}/A_0$) is dependent on energy-transfer mechanisms. Fortunately, a one-to-one correspondence can be derived between the conical semiangle and A_0 (fig. 9) assuming that the ensemble of donors are uniformly distributed throughout the cone. For an unconstrained donor, $A_0 = 0.4$, while for small θ_c, the limiting anisotropy approaches 1. The assumption of uniform distribution corresponds to the hard-cone potential. In the presence of an angular dependent potential, we expect the dipoles to assume a Boltzmann distribution, and the correspondence between θ_c and A_0 will differ from fig. 9.

Previous studies have related the decay of the anisotropy to the magnitude of the wobbling diffusion constant. As energy transfer will influence the anisotropy decay, the analysis is no longer straightforward. The anisotropy decay curves for cases 1–4 are presented in fig. 10. We again note the competition between diffusive processes tending to equilibrate the distribution, and energy-transfer processes which act to select a preferred alignment. The form of the anisotropy decay curve and the value of $A_{\lim}$ are determined by both rotational diffusion and energy transfer. Much information is contained in the anisotropy curve,

however, at this time, no theory exists by which to interpret these measurements.

5. Conclusions

Dale and Eisinger [5] considered two time regimes for energy transfer. First, the dynamic regime where the relative motion of the donor and acceptor is fast compared to the energy-transfer rate and the donor lifetime. The dynamic average of the transfer rate is computed by assuming that each donor-acceptor pair samples all available configurations during the measurement. Second, the static regime where each donor-acceptor pair is assumed to be in a single configuration, but the ensemble of donor-acceptor pairs assumes all available configurations. In both cases, $\langle k^2 \rangle$ is constant, and can be calculated.

Simulation techniques are most useful when $\langle k^2 \rangle$ is a function of time. This criterion excludes both the dynamic and static regime, but includes the intermediate case which might be of greatest value for intramolecular dynamical measurements. In a depolarization experiment, a time-dependent $\langle k^2 \rangle$ implies that the photoselected dipoles can evolve significantly from the initial photoselected distribution. It was noted that when a time-dependent $\langle k^2 \rangle$ is coupled with an efficient energy-transfer process, a nonexponential luminescence decay is observed.

Luminescence decay measurements are useful for quantifying the energy-transfer rate constant. If the donor and acceptor are rigidly fixed at known orientations, then R_{DA} can be deduced. Alternatively, if the donor-acceptor separation is known, then the orientation factor can be determined. A completely unknown donor-acceptor configuration will further confound interpretation; a short distance coupled with an inefficient alignment is indistinguishable from a better aligned pair at greater separation. In addition, orientational freedom will further contribute to ambiguity.

The power of depolarization measurements to resolve configurations of equal energy-transfer efficiency has been discussed in terms of an intrinsic photoselection brought on by the acceptor species. Further, both depolarization and repolarization effects were observed in our simulation, and the time course of the anisotropy was understood as a competition between diffusive and dissipative processes.

The limitations of our model must be kept in mind. Firstly, we have assumed the absorption and emission moments of the donor to be colinear. This assumption simply influences the value of A_0 in a predictable way. Secondly, we have assumed the acceptor to be rigidly fixed, an accurate depiction of many biological macromolecules (for example, the heme in hemoproteins). Lastly, by neglecting macromolecular tumbling and requiring the donors to wobble in the neighborhood of an axis parallel to the z-axis, we assume an oriented sample.

In this work, we have considered simple systems in order to interpret our results most readily, however, the robustness and flexibility of our simulation allow for routine modification.

Acknowledgements

This work was supported by an NIH Cell and Molecular Biology Training Grant (J.W.B.) and NIH grant GM21487 (J.M.V.).

References

1 L. Stryer, Annu. Rev. Biochem. 47 (1978) 819.
2 T. Forster, Ann. Phys. 2 (1948) 55.
3 R.E. Dale and J. Eisinger, Biopolymers 13 (1974) 1573.
4 R.E. Dale, J. Eisinger and W.E. Blumberg, Biophys. J. 26 (1979) 161.
5 R.E. Dale and J. Eisinger, in: Biochemical fluorescence concepts, vol. 1, eds. R.F. Chen and H. Edelhoch (Marcel Dekker, New York, 1975) p. 115.
6 F. Perrin, J. Phys. Radium 5 (1934) 497.
7 F. Perrin, J. Phys. Radium 7 (1936) 1.
8 G. Weber, Biochem. J. 51 (1952) 145.
9 L.D. Favro, Phys. Rev. 119 (1960) 53.
10 T. Tao, Biopolymers 8 (1969) 609.
11 G.G. Belford, R.L. Belford and G. Weber, Proc. Natl. Acad. Sci. U.S.A. 69 (1972) 1392.
12 R.F. Steiner, in: Excited states of biopolymers, ed. R.F. Steiner (Plenum Press, New York, 1983) p. 117.
13 K. Kinosita, S. Kawato and A. Ikegami, Biophys. J. 20 (1977) 289.

14 K. Kinosita, A. Ikegami and S. Kawato, Biophys. J. 37 (1982) 461.
15 G. Lipari and A. Szabo, J. Chem. Phys. 75 (1981) 2971.
16 T. Fujiwara and K. Nagayama, J. Chem. Phys. 83 (1985) 3110.
17 A. Szabo, J. Chem. Phys. 81 (1984) 150.
18 C.R. Cantor and P.R. Schimmel, Biophysical chemistry, part II (W.H. Freeman, San Francisco, 1980).
19 K. Sharp, R. Fine, K. Schulten and B. Honig, J. Phys. Chem. 91 (1987) 3624.
20 Z. Schuss, Theory and application of stochastic differential equations (Wiley, New York, 1980).
21 S.A. Allison, S.H. Northrup and A. McCammon, Biophys. J. 49 (1986) 167.
22 W. Nadler, A.T. Brunger, K. Schulten and M. Karplus, Proc. Natl. Acad. Sci. U.S.A. 84 (1987) 7933.
23 S. Lee, M. Karplus, D. Bashford and D. Weaver, Biopolymers 26 (1987) 481.
24 K. Sharp, R. Fine and B. Honig, Science 236 (1987) 1469.
25 M.C.L. Martinez and J.G. de la Torre, Biophys. J. 52 (1987) 303.
26 F. Tanaka and N. Mataga, Biophys. J. 39 (1982) 129.
27 T.G. Dewey and G.G. Hammes, Biophys. J. 32 (1980) 1023.
28 H. Kellerer and A. Blumen, Biophys. J. 46 (1984) 1.
29 P.K. Wolber and B.S. Hudson, Biophys. J. 28 (1979) 197.
30 B. Snyder and E. Freire, Biophys. J. 40 (1982) 137.
31 D. Ermak and J.A. McCammon, J. Chem. Phys. 69 (1978) 1352.
32 S.C. Harvey and H.C. Cheung, Proc. Natl. Acad. Sci. U.S.A. 69 (1972) 3670.
33 J.B. Marion, Classical dynamics of particles and systems (Academic Press, New York, 1970).
34 E.R. Henry and R.M. Hochstrasser, Proc. Natl. Acad. Sci. U.S.A. 84 (1987) 6142.
35 S.M. Janes, G. Holtom, P. Ascenzi, M. Brunori and R.M. Hochstrasser, Biophys. J. 51 (1987) 653.